Journal of
Ceramic Science
and Technology

J. Ceram. Sci. Technol., 09 [4] 381-390 (2018)
DOI: 10.4416/JCST2018-00024
available online at: http://www.ceramic-science.com

Novel Cement-Ceramic Encapsulation Material for Electronic Packaging

S. Kaessner*[1, 2], N. Wichtner[1], F. Hueller[3], C. Berthold[1], K. G. Nickel[1]

[1]University of Tuebingen, Geosciences, Applied Mineralogy, D-72074 Tuebingen, Germany
[2]Robert Bosch GmbH, Corporate Sector Research and Advance Engineering, D-71272 Renningen, Germany
[3]Friedrich-Alexander University Erlangen-Nuernberg (FAU), GeoZentrum Nordbayern, Mineralogy, D-91054 Erlangen, Germany
received March 12, 2018; received in revised form April 16, 2018; accepted May 29, 2018

Abstract

Future power electronic devices with high power density and reduced chip area need robust encapsulation materials with increased thermal conductivity and temperature stability. Especially for new SiC and GaN semiconductor technology, operating temperatures above 200 °C can increase the potential of future power electronics. This paper introduces a novel uniquely processed cement-ceramic composite material for electronic packaging, containing a calcium aluminate cement (CAC) matrix and high amounts of alumina fillers. In-situ μ-XRD²-DTA, where X-ray diffraction patterns and DTA traces can be monitored simultaneously, was applied to investigate the dehydration behavior of this composite between room temperature and 300 °C for the first time. The results reveal the high potential of using in-situ μ-XRD²-DTA for measurements on cement-ceramic composites. The observed microstructure evolution shows micro-crack formation and increased porosity above 210 °C, which can be correlated with the dehydration of gibbsite and katoite. At this stage, the novel cement-ceramic encapsulation material already enables miniaturized passive electronic components. Further consequences for electronic packaging of semiconductors and correlations to state-of-the-art encapsulation materials are discussed.

Keywords: Cement-ceramic encapsulation, CAC, processing, dehydration, electronic packaging

I. Introduction

With increasing power density and reduced chip area, power electronics need robust and thermally conductive encapsulation. Especially for future power electronics, application temperatures up to nearly 300 °C, enhanced lifetime, reliability, robustness and integration are major issues in current research work [1–4].

Typical encapsulation materials like silicone gels or filled epoxy resins show limited thermal conductivity, higher thermal expansion and need special processing conditions for proper gap filling and workability. In addition, epoxy resins generally have a glass transition temperature (T_g) within the operating temperature regime, which leads to degradation and crack formation. Due to their high coefficient of thermal expansion (CTE), CTE-mismatches within the electronic package can cause thermomechanical stress and limited reliability, especially in power electronic applications. Furthermore, most epoxy resins are not stable beyond 180 – 200 °C. First investigations revealed that μm-scaled cement-ceramic composites, specially cured at temperatures between 60 and 80 °C, show great promise for better thermal and processing properties in contrast to filled epoxy resins or silicone gels. Table 1 exemplarily illustrates selected properties of a commercially available silicone gel and filled epoxy resin for electronic potting, compared to the developed cement-ceramic encapsulant. It clarifies the advantages of the novel self-flowing encapsulant, such as high thermal conductivity and processing in which specific temperature or pressure is not needed for the encapsulation process.

The cement-ceramic encapsulation material is similar to refractory concrete with calcium aluminate cement (CAC) as the hydraulic binder phase. However, those concretes are sintered at high temperatures to create a mechanically stable binding, while the developed encapsulant is treated at temperatures below 100 °C. Furthermore, the grain size of alumina is typically below 50 μm, which puts this new encapsulant close to nano-concrete from treated Portland cement and sand. With consideration of all of these aspects, the presented material rather resembles a uniquely processed cement-ceramic composite, in which the grain boundary phase has been replaced by the set hydraulic phase, similar to cast stone. Thus, it can be described as a hybrid type of composite and is named 'CAC ceramic composite' (CCC).

* Corresponding author: stefan.kaessner@de.bosch.com

Table 1: Selected material and processing properties of a commercially available filled epoxy resin and silicone gel (data from technical data sheets), compared to the developed cement-ceramic encapsulant.

	Filled Epoxy Resin[a]	Silicone Gel[b]	Cement-Ceramic Encapsulant[c]
Thermal expansion [ppm/K]	8/38 (> 135 °C)	1000	4 – 12
Glass transition [°C]	135	-	-
Thermal conductivity [W/(mK)]	1	0.17	> 5
Volume resistivity [Ohm cm]	10^{11}	10^{15}	10^{8}
Processing	Transfer molding 175 – 180 °C, 70 – 120 x 10^5 Pa	Room temperature and vacuum	Room temperature (± vacuum)

[a] Sumitomo Bakelite, Sumikon EME-G770HE, [b] Momentive, TSE 3062, [c] Laboratory data (Robert Bosch GmbH)

The developed CCC addresses all important aspects due to the intrinsic properties, such as the high thermal conductivity above 5 W/(mK) and better workability at ambient conditions. The CCC consists of an iron-free calcium aluminate cement (CAC) matrix and alumina, which acts as the ceramic filler. In contrast to conventional organic encapsulants, this material hardens via a cement hydration reaction. Calcium aluminate cement usually forms metastable phases, which convert to stable phases under volume change. Mechanical instability is the result and the use of CAC for building constructions has not been allowed since 1962 in Germany [5–11].

Owing to the specific hardening above 60 °C, the developed CAC ceramic composite overcomes these problems and forms directly stable hydrate phases that do not show any conversion reactions. The finally hardened CCC acts then as a non-deformable encapsulation material for any type of electronic.

CAC in combination with alumina is mainly used for refractories and part of according research work [12–16]. In contrast to CCC, the hydrated CAC is sintered during the application as refractory material to obtain a ceramic bonding. Applications where CAC are not sintered at the end are generally not present in the ceramic or refractory research field. CAC is mostly used for special applications, cement chemistry and for repair work, besides refractories due to its fast setting, chemical and thermal resistance [17]. Unlike CCC, the material composition of a composite-containing CAC and common concrete additives is very different in respect of particle sizes, chemical composition or amount of feedstock and hydration conditions.

As pointed out, the type of CAC ceramic composite (CCC) introduced in this paper represents a new encapsulation material for electronic packaging. In order to understand phase reactions and thermal behavior, the CCC was investigated to determine its microstructural features, phase evolution during dehydration and the corresponding change in porosity for the first time. Especially due to the variety of different results on dehydration of CAC hydrate phases, the results are of significant importance.

To analyze the microstructure, SEM with advanced preparation techniques were applied and porosity was measured with mercury intrusion porosimetry (MIP). The dehydration behavior of the CCC was analyzed with a new method of connecting DTA and XRD in in-situ monitoring called 'in-situ μ-XRD²-DTA' [18], which helped to understand the material during processing and application at temperatures up to 300 °C. XRD quantitative analysis with two different methods was used to obtain proper phase contents.

The chemical compositions cited in this paper are written in accordance with CAS notation where C = CaO, A = Al_2O_3 and H = H_2O.

II. Experimental Procedure

For all investigations on CCC, alumina and CAC raw materials were dry mixed in a ratio of 4:1 (wt%). In a second step, de-ionized water (water to cement ratio of 0.55), a dispersant and a defoaming agent were homogenized with the prepared raw materials in a vacuum-stirrer at 300 rpm to achieve a castable slurry. Finally, the slurry hardened in a closed 10-mm cylindrical casting mold in a drying chamber at 60 °C for 6 h. Further sample preparation for each of the analytical methods will be described in the appropriate paragraphs.

For SEM analysis, the samples were ion-etched and sputtered after a dry grinding and polishing process. Ion etching is preferred over conventional preparation techniques, because the CCC should have no contact with water during sample preparation, as it could change the microstructure by continued hydration. Additionally, standard SEM preparation would partially fill the pores with abraded material. SEM images and EDX-mappings were obtained on a Zeiss Supra 35VP with INCA Energy EDS-System from Oxford Instruments.

Applying MIP (Mercury Intrusion Porosimetry) for the investigations on pore structure makes a possible change in pore volume due to dehydration detectable. Furthermore, SEM pore analysis alone is not applicable, as the pore sizes vary too much for a clear description in a proper number of images. Therefore, 4 – 5 g of hardened CCC were measured on a Thermo Scientific porosimeter up to 400 MPa. To identify changes in microstructure or porosity of CCC, each of the measurements (SEM and MIP) were performed at room temperature without tempering and after 12 h of tempering at 150 °C and 300 °C, respectively.

For quantification of the crystalline phase content, measurements were conducted with a Bruker D8 Advance X-

ray diffractometer at 40 kV /20 mA from 10 – 90° 2θ with a measurement time of 68 minutes. A setup with a Cu-sealed tube, a Göbel mirror, a cutting slit and 0.2° divergence slit on the primary site and a VÅNTEC-1 detector provided 0.4 s per step with 0.008° increments for reasonable count statistics. Quantitative phase contents were calculated via Rietveld refinement with SiroQuant 4.0 Software using the implemented structure data of the software. For all XRD measurements, CCC samples were analyzed on untreated surfaces.

Comparatively, in cooperation with the Institute for Mineralogy of the University of Erlangen-Nuernberg, a machine-cut sample of CCC was measured on a Bruker D8 Advance X-ray diffractometer at 40kV/40 mA from 6 – 70° 2θ with a measurement time of 46 minutes. A setup with Cu-sealed tube, 0.3° divergence slit and a Lynx-Eye detector providing 1 s per step with 0.0236° increments was applied for quantification with the G-factor method using ICSD structure data [19,20].

The method of coupling X-ray diffraction and thermal analysis allows the straight connection of both XRD and DTA results. With separate, thus uncoupled systems, a direct correlation of results is difficult owing to differing measurement conditions such as sample preparation, etc.

For in-situ-coupled μ-XRD²-DTA measurements, a Bruker D8 DISCOVER GADDS X-ray microdiffractometer (μ-XRD²) was used. The system was equipped with a Co-sealed tube, a primary HOPG-monochromator, a monocapillary optic with a spot size of 500 μm (FWHM) and a large two-dimensional VÅNTEC-500 detector, covering ~40° 2θ in one measurement (XRD²).

This μ-XRD² setup allows very short measurement times with a high spatial resolution due to the high flux and the small spot size provided by the monocapillary optic. The large two-dimensional detector enables the monitoring of dehydration, crystallite ripening or texture effects in real-time without detector movement. Hence, it is possible to measure a diffraction pattern with reasonable count statistics covering ~40° 2θ and ~40° ψ within 10 seconds.

The DTA-setup with an in-house designed DTA-chamber is shown in Fig. 1 and allowed constant heating and cooling of the sample [18]. The sample holder itself was covered by a small lid to avoid disturbing influences on the DTA-signal caused by thermal convection of the surrounding air. The lid's window is transparent to X-rays and does not restrict the covering range of the two-dimensional detector.

As the in-situ-coupled μ-XRD²-DTA setup is equipped with a humidity sensor, correlation between DTA trace, relative humidity, absolute humidity and the corresponding phase content of the sample is possible.

Measurements on CCC were performed with a Co-sealed tube operating at 40 kV /40 mA, fixed incident angle $\theta_1 = 12°$, fixed detector angle θ_2 for covering a range from 17 – 54° 2θ, 120 s measurement time for each diffraction pattern and 5 K/min heating and cooling rates of the sample. Polished CCC samples measuring 0.5 mm in thickness and 10 mm in diameter were prepared to fit the sample holder. The diffraction patterns were captured consecutively: Once an integration time was finished, a new measurement started automatically. The dead time between two measurements averaged three seconds.

III. Results

Fig. 2a gives a brief overview of the microstructural features of CCC, showing the hydrated CAC matrix, providing the mechanical strength with calcium aluminate hydrate (CAH) and aluminate hydrate (AH) phases. Additionally, small amounts of unhydrated CAC clinker phases and small pores are visible. Alumina particles with different particle sizes for best packaging density, achieved in accordance with [21], are used as thermally conductive fillers. Figs. 2b+c illustrate an area of interest and the correlating EDX-mapping of a CCC. With plotting of the Ca and Al elements, it is useful to differentiate between unhydrated (green) and hydrated (red) areas, as the clinker phases contain on average higher amounts of Ca.

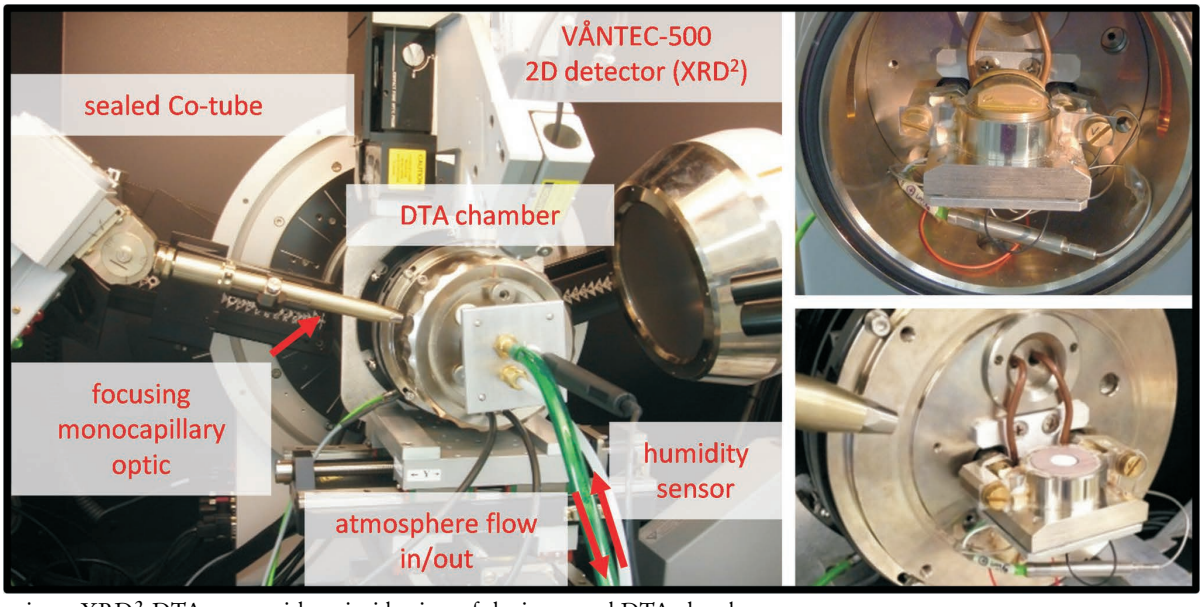

Fig. 1: In-situ μ-XRD²-DTA setup with an inside view of the improved DTA chamber.

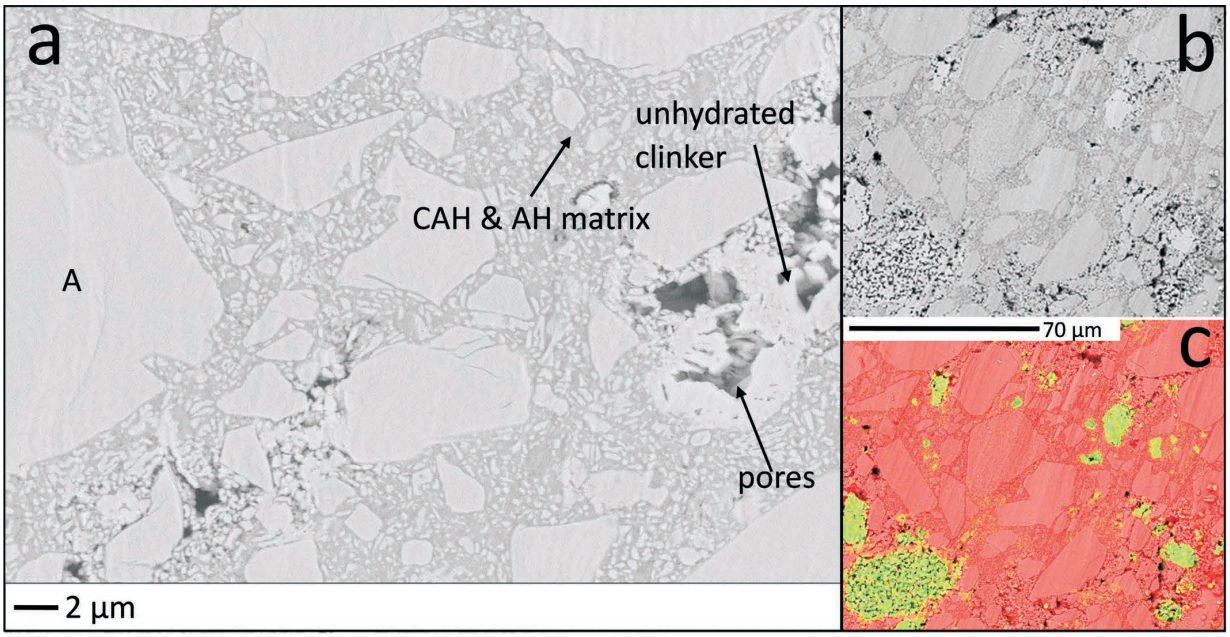

Fig. 2: Microstructure of a CAC ceramic composite (CCC) (a) a selected area of interest (b) with the corresponding EDX-mapping of Ca (green) and Al (red) (c), plotted for differentiating between unhydrated cement clinker and matrix + alumina filler.

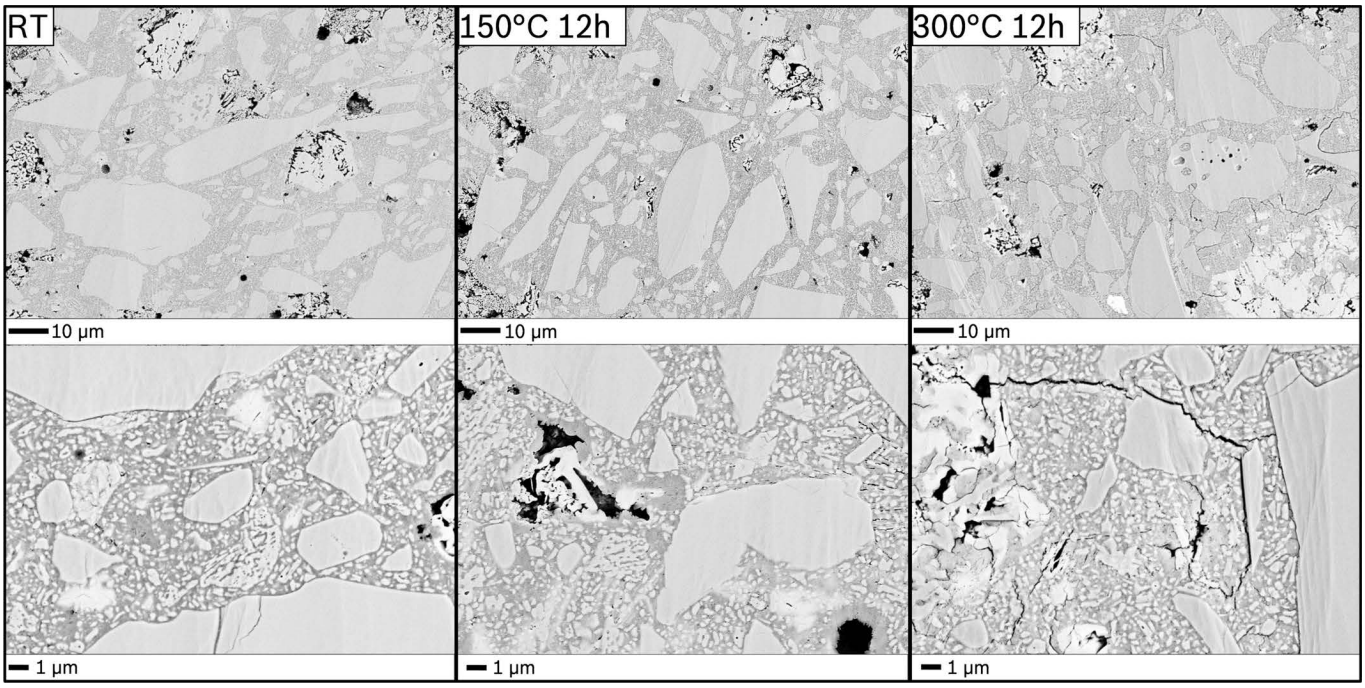

Fig. 3: Typical CCC microstructure; at room temperature (RT), after tempering at 150 °C and after tempering at 300 °C.

Concerning the pore structure, it is obvious that pore sizes range from the nm to µm scale, while most of the bigger pores accumulate at the unhydrated CAC clinker phases. To evaluate the influence of dehydration on the microstructure of a CCC, Fig. 3 shows the SEM images of the same CCC without tempering, after tempering for 12 h at 150 °C and after tempering for 12 h at 300 °C. The composite microstructure does not change until 150 °C. After tempering at 300 °C, a significant micro-crack formation leads to damage within the matrix.

The pore volume of the CCC was quantified at room temperature (RT), 150 °C and 300 °C by means of MIP (Mercury Intrusion Porosimetry). The results shown in Fig. 4 give evidence that the pore volume increases between 150 °C and 300 °C. For better visibility, the results are also given in accessible porosity in vol%, which is calculated in accordance with the skeleton density measured with He-pycnometry. Thus, an increase of about 5 vol% accessible porosity after tempering at 300 °C can be observed. Values at RT and after tempering at 150 °C are similar. This fact correlates to microstructure development as shown in Fig. 3. Therefore, the increase in porosity correlates with the observed micro-crack formation. The XRD results provide reasons for this micro-crack formation.

As mentioned before, CCC consists of different crystalline phases including alumina for advanced thermal conductivity. Especially for a robust electronic encap-

sulation material, it is important to know which of the possible hydrate phases are present in the matrix, because conversion of metastable hydrates, as described in the introduction, would lead to volume changes. Fig. 5 identifies the present phases at RT, after tempering for 3 h at 150 °C and after tempering for 3 h at 300 °C. With these three diffraction patterns it is possible to quantify what should be observed in an in-situ μ-XRD²-DTA measurement concerning phase content and amount.

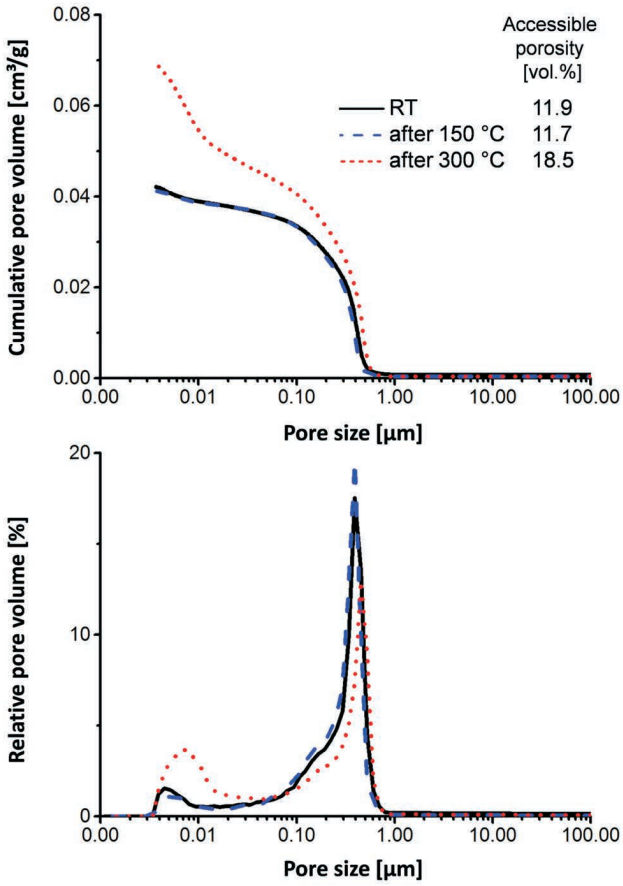

Fig. 4: Mercury intrusion porosimetry (MIP) data of a CCC at room temperature (RT), after tempering at 150 °C and after tempering at 300 °C.

CCC can be characterized by a matrix of gibbsite (γ-AH_3) and katoite (C_3AH_6) with corundum (α-A) filler and small amounts of unhydrated cement clinker, such as krotite (CA) and grossite (CA_2) (Fig. 5 at RT). A comparison of the three XRD patterns shows that the phase content does not change after 150 °C tempering. Only from 150 to 300 °C complete dehydration destroys all hydrate phases and a new phase $C_{12}A_7$, known as a CAC clinker phase, appears. Complete dehydration of the cement matrix leads to the observed micro-crack formation and porosity increase in this temperature regime.

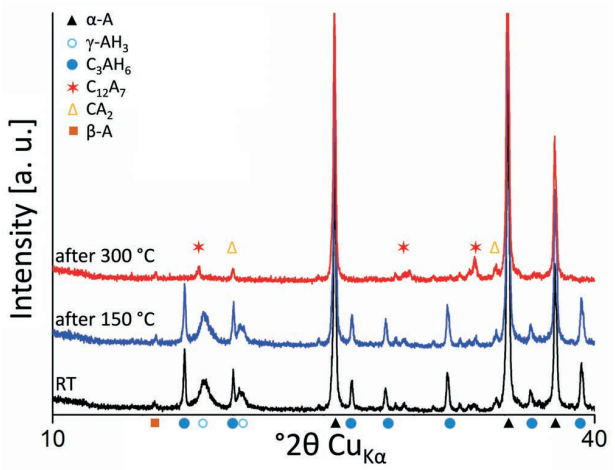

Fig. 5: Ex-situ XRD measurements for phase quantifications at room temperature (black), after tempering at 150 °C (blue) and after tempering at 300 °C (red).

Quantification results, achieved with SiroQuant 4.0 Software via Rietveld refinement, are shown in Table 2. A cross-check with XRD quantifications via G-factor method validated these results (as presented in Table 2) with only slight differences for hydrate phases and clinker amount. Furthermore, we found out that nearly all mixing water (water to cement ratio (w/c) = 0.6) is incorporated into hydrate phases taking the mineralogical composition, amount of CAC and the following hydration reactions into account:

$$3CA + 12H_2O \rightarrow C_3AH_6 + 2\gamma\text{-}AH_3 \quad (1)$$

$$3CA_2 + 21H_2O \rightarrow C_3AH_6 + 5\gamma\text{-}AH_3 \quad (2)$$

Table 2: Calculated crystalline phase contents of CAC-Ceramic Composite (CCC) after Rietveld Refinement between 10 and 40 °2θ (errors within digit). The last column shows quantification results obtained with G-factor analysis for comparison.

Mineral name	CAS notation	Amount [wt%]			
		RT	150 °C	300 °C	RT G-factor
Corundum	α-A	72.8	73.3	89.1 ± 0.1	75 ± 1.9
Gibbsite	γ-AH_3	13.5	12.9	-	15.8 ± 0.3
Katoite	C_3AH_6	8.9	8.0	-	9.6 ± 0.1
Diaoyudaoite	β-A	1.7	1.9	3.5	1.2 ± 0.2
Krotite	CA	< 1	< 1	-	< 1
Grossite	CA_2	3.1	3,6	4.8	< 1
Mayenite	$C_{12}A_7$	-	-	2.6	-

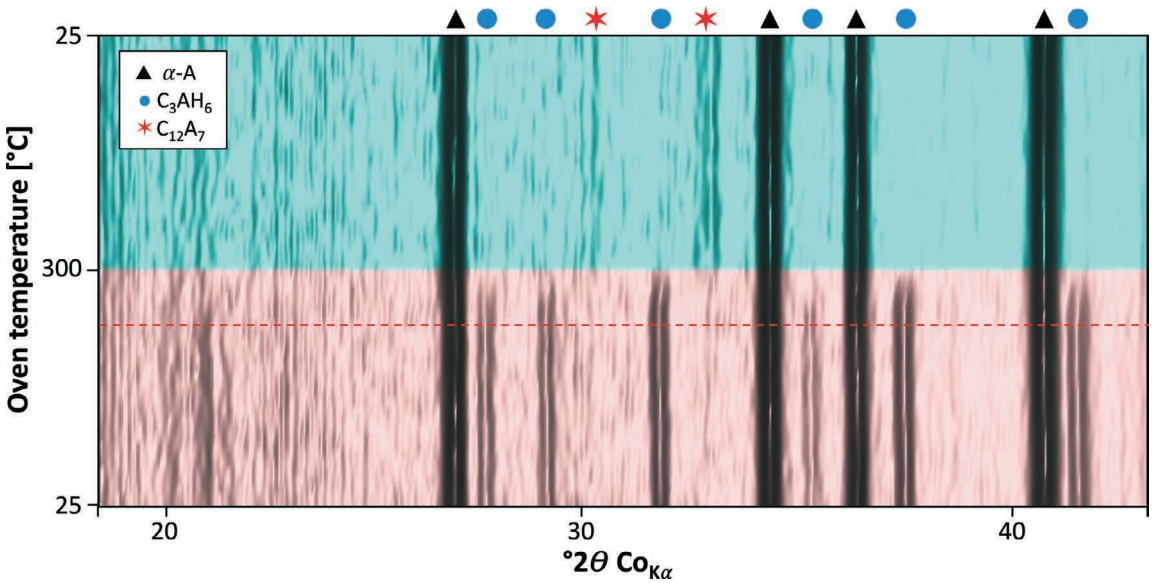

Fig. 6: 2D-plot of the phase evolution of a CCC during heating and cooling, measured with in-situ µ-XRD²-DTA.

Fig. 6 illustrates the result of the in-situ µ-XRD²-DTA measurements concerning the phase evolution during heating to 300 °C and subsequent cooling. Owing to the short measurement times, it is not possible to differentiate between γ-AH_3 and C_3AH_6 during the experiment. Nevertheless, taking Fig. 5 and the C_3AH_6 peak evolution into account, dehydration starts above 150 °C for both phases. The CCC dehydration occurs starting from a temperature of about 210–220 °C, resulting in the formation of $C_{12}A_7$ as reported in [22]. Thus, X-ray diffraction alone is not sufficient for the determination of the exact starting temperature of the dehydration.

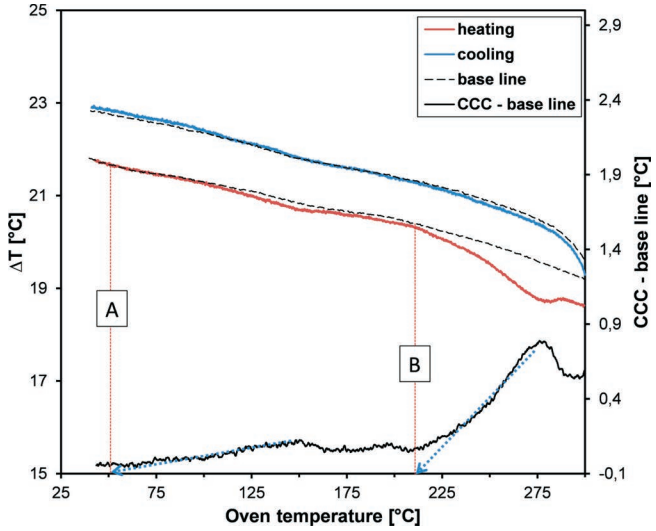

Fig. 7: DTA trace (red) measured with in-situ µ-XRD²-DTA. Points A and B indicate the extrapolated starting temperature T_e of the two observed endothermic reactions (black). The dashed line gives the base line.

In addition, the extrapolated starting temperature (T_e), giving reasonable values for the start of a reaction from DTA traces, was identified by subtracting the base line from the DTA trace. The tangent of the inflection point was extrapolated to the base of each reaction peak mark T_e. Correlating the phase evolution with the simultaneously measured DTA trace proves a T_e of 210–220 °C for the start of dehydration (Fig. 7 - point B). This type of reaction is endothermic.

Previously, another endothermic reaction occurred between RT and the dehydration of hydrate phases (Fig. 7 – point A). Unfortunately, it is not possible to determine a certain temperature for this first dehydration, due to the broad peak of this endothermic reaction. Nevertheless, there is no phase transformation in this first temperature regime present in the simultaneously recorded X-ray patterns (see Fig. 6). It is also important to notice that during cooling no reaction occurs. Thus, CCC dehydration is irreversible. XRD analysis of CCC samples that were tempered at 300 °C and subsequently stored for a few weeks at ambient conditions verified this fact. Therefore, we used the second measurement of the same sample as the DTA base line.

Finally, it is obvious that the progress of relative and absolute humidity changes slopes significantly at the same temperatures of the DTA trace (Fig. 8 - points A and B). Therefore, changes in humidity indicate dehydration processes in CCC. The impact of different humidity values on the phase evolution of CAC ceramic composites will be evaluated in future studies.

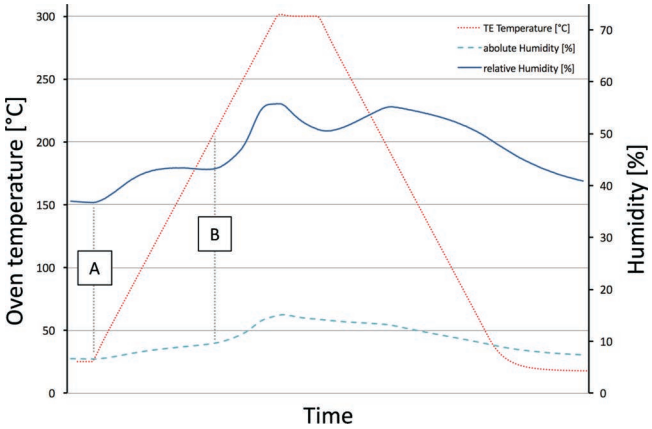

Fig. 8: Humidity values from the in-situ µ-XRD²-DTA measurement plotted with the temperature of the thermoelement (TE) (dashed red) also named as oven temperature. Points A and B correlate with T_e indicated in Fig. 7.

IV. Discussion

1. *Microstructure*

SEM images show that a dry grinding and polishing process combined with ion etching is a suitable preparation technique for CCC, as they do not destroy any feature of the microstructure. Neither crystalline phases, nor pores are adversely affected in a negative way, even in the nm scale. Nevertheless, pore areas have to be evaluated carefully, due to redeposition effects, which can occur after ion etching.

Concerning EDX-Mapping on CCC samples, it has to be pointed out that a distinction between matrix and fillers or in some areas between CA and CA_2 clinker is limited. This fact results from the EDX resolution being too low combined with the very fine-grained microstructure of CCC. Further research with advanced detector and SEM equipment may improve quantitative microstructure analytics on CCC.

All changes in the microstructure of CCC occurred between 150 °C and 300 °C. The results mainly correlate with observations in CAC-based materials. Nevertheless, it is reported for the first time for the uniquely processed µm-scaled material. Hence, for the use as an encapsulating material for electronic packaging the behavior in this particular temperature regime will be very interesting. Relevant material properties, like electrical resistance or mechanical strength, will change, because porosity increases by about 5 vol% and because micro-crack formation occurs above 150 °C. Especially the open porosity as described in cement literature leads to permeability and hygroscopic effects [23,24].Finally, the dehydration behavior (as discussed in-depth in IV.2) will have an impact on functionality and further development of these cement-ceramic encapsulation materials.

2. *Dehydration behavior*

In-situ coupled µ-XRD²-DTA and ex-situ XRD results are in good agreement with the observed temperature-dependent changes in microstructure. Complete dehydration of the CCC starts at about 210 – 220 °C (see Fig. 6 and Fig. 7), a temperature regime where also porosity changes and micro-cracks occur. Therefore, both effects (increased porosity and micro-crack formation) can be correlated with dehydration at 210 – 220 °C and the smaller volume of dehydrated phases in the composite. Rouquerol et al. support this correlation, as they found out that dehydration of gibbsite increases its porosity [25].

For gibbsite, the main hydrate phase of CCC, thermal decomposition has been studied for decades, since it is of importance for the Bayer-process and the alumina production. In general, gibbsite transforms to either boehmite or directly to χ-Al_2O_3 with the release of water, which depends on time, water vapor pressure of the atmosphere and grain size. That is the reason for the variety of different temperature regimes reported for the dehydration of gibbsite. Fine-grained gibbsite for example dehydrates directly to χ-Al_2O_3 at 280 – 300 °C with rapid heating, while hydrothermal conditions cause a reaction to boehmite at 300 °C. Together with results, which consider a decomposition of gibbsite starting at 140 °C, a temperature regime from 140 to 350 °C is conceivable [22,26,27]. The DTA traces of the stable, converted CAC paste from Rouquerol (illustrated in Fig. 9) show trends of endothermic reactions similar to our CCC (measured with in-situ µ-XRD²-DTA). However, they disregard the first (blue) section, where the gibbsite dehydration should already start. Adding all sections to both DTA traces, a correlation to CCC could identify a gibbsite dehydration from 210 °C to 280 °C and a katoite dehydration from 280 °C to 300 °C.

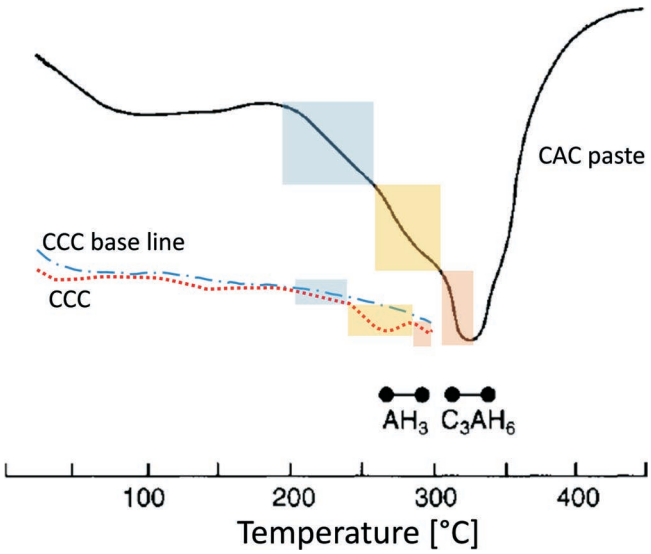

Fig. 9: DTA traces of CAC paste (DTA) and CCC (in-situ µ-XRD²-DTA) (after Newman and Choo [24]).

Evaluating the complete method of in-situ µ-XRD²-DTA, a general offset, XRD-to-DTA offset and a mismatch of about 10 °C due to measurement times of 120 s with a ramp rate of 5 K/min. have to be taken into account. Therefore, it can be assumed that dehydration starts a little bit earlier at about 180 – 200 °C. DSC and TG-MS measurements of the same CCC support this assumption and CCC dehydration starting between 180 – 200 °C is in agreement with the discussed literature of the previous passage.

Furthermore, Fig. 6 reveals the end of dehydration (for both phases: gibbsite (γ-AH_3) and katoite (C_3AH_6)) at about 300 °C, which finally spans a temperature regime from 180 to 300 °C for the complete dehydration of both CCC hydrate phases. As Fig. 7 and Fig. 8 show complete gibbsite and katoite dehydration, starting above 200 °C (Point B), one more endothermic reaction is visible (Point A). This reaction starts above RT and can be correlated to the removal of free water, which needs more energy depending on time and pore size.

In contrast to materials containing significant amorphous amounts, the comparison of quantification via the G-factor method and Rietveld refinement showed no significant difference in phase contents for the CCC (Table 2). The slightly different amounts of CA and CA_2 correlate with heterogeneity, which can be observed in the microstructure of CCC (Fig. 2 and Fig. 3). The difference of about 3 wt% for gibbsite (see RT vs. RT G-factor in Table 2) is still in the error range of such a CCC, because quantification of the same material on different spots resulted

in about 16 wt% of gibbsite. Furthermore, the crystallinity of gibbsite is quite low and different structure models were used, which might also lead to different quantification results. Therefore, both methods are suitable to determine the quantitative phase content of a CAC ceramic composite.

3. Consequences for electronic packaging

Taking all aspects of IV.1 and IV.2 into account, the developed cement-ceramic encapsulation material (CCC) can be applied for passive electronic components (coil or transformer) with reduced size and high power density already at this stage of development. These components operate at low temperatures up to 150 °C and should not cause any dehydration or microstructural changes in CCC. Additionally, first over-voltage and thermal resistance tests on passive components support this assumption.

Si semiconductors encapsulated with CCC operating at about 180 – 200 °C should also not influence the microstructure or phase content of the encapsulant. Although, the lower volume resistivity of CCC (see Table 1) has to be considered in terms of electronic isolation and reliability. Therefore, current investigations on ion-migration and chemical interactions between CCC and the chip surfaces will identify the mechanisms for possible enhancements or limitations with the application of CCC encapsulation material. Qualification tests, like measuring the influence on surface insulation resistance (SIR) [28] and reverse bias under high temperature and humidity (HTRB and H³TRB) [29, 30, 31] are therefore part of ongoing research work. Also power cycling tests (PC), simulating the real use condition of electronic devices, will be conducted [29]. Thus, it is possible to evaluate the reliability of the composed electronic system by repeatedly turning the devices on and off under defined conditions, until the end of life.

The applicability of CCC on wide bandgap semiconductors like SiC or GaN above 210 °C have to be evaluated in terms of measures against reliability issues by dehydration or porosity. Therefore, above-mentioned qualification tests should reveal critical aspects for wide bandgap power electronic devices.

V. Conclusions

With coupled measurements of DTA and μ-XRD² and the needed time and temperature resolution, it was possible to observe the irreversible dehydration process of the presented cement-ceramic encapsulation material for the first time. These data correlate with the observations on porosity and microstructure evolution up to 300 °C. Furthermore, in-situ μ-XRD²-DTA revealed a stable system up to nearly 180 – 200 °C. Beyond this temperature, dehydration and increased porosity by micro-crack formation have to be considered in CCC development for electronic applications in this temperature regime.

Future electronic devices equipped with SiC or GaN semiconductors and small passive components with increased power density and heat stresses, need a robust and highly thermally conductive encapsulation compound. The developed calcium aluminate cement ceramic composite introduces a new material class, which exhibits enhanced thermal properties and simplified processing compared to common filled epoxy resins or silicone gels. The μm-scaled material and its special processing above 60 °C overcome the known problems associated with conversion in CAC-based systems, by means of immediate formation of stable hydrates.

Therefore, evaluating electrical, chemical and thermo-mechanical aspects of CCC is part of current research. Especially, typical qualification tests under distinct atmospheric conditions with different humidity and temperature (SIR, HTRB, H³TRB and PC) will be considered and compared to state-of-the-art encapsulants.

Beside all advantages of the novel cement-ceramic encapsulation material, the discussed results revealed critical aspects for the application on semiconductors and at temperatures above 210 °C. Finally, the correlation between quantitative phase content, electrical and thermo-mechanical properties has to identify the key parameters for future electronic packaging with CAC ceramic composites and the role of CCC in the ceramic research community.

Acknowledgement

We would like to thank Robert Bosch GmbH and its corporate research sector, where the CAC ceramic composite (CCC) has been developed during the doctoral study of Stefan Kaessner. Especially we express our gratitude to Georg Hejtmann and his CR/ARM2 project team for supporting and discussing this work. We are very thankful for the financial support by Germany's Federal Ministry of Education and Research and the granted publicly financed project "ReLEEB" (16EMO0223K).

For the help and development of advanced preparation processes for CCC microstructure analysis, we like to mention the great work of Ulrike Taeffner and Ingrid Wuehrl from the Corporate Analytics at Robert Bosch GmbH. For the successful completion of this paper, we also appreciated the helpful advice of the reviewers.

Finally, we want to thank Prof. Thomas A. Bier and Sandra Waida for MIP measurements on the CCC and for sharing their knowledge on CAC.

References

1 Ohara, K., Masumoto, H., Takahashi, T., Matsumoto, M., Otsubo, Y.: A New IGBT Module with Insulated Metal Baseplate (IMB) and 7th Generation Chips. In: Proceedings of PCIM Europe 2015. Nuremberg, Germany, 2015.

2 Asada, S., Kondo, S., Kaji, Y., Yoshida, H.: Resin Encapsulation Combined with Insulated Metal Baseplate for Improving Power Module Reliability. In: PCIM Europe 2016. Nuremberg, Germany, 2016.

3 Stosur, M., Sowa, K., Piasecki, W., et al.: Encapsulation of power electronics components for operation in harsh environments, Arch. Electr. Eng., **66**, [4], 855 – 866, (2017).

4 Yao, Y., Lu, G.-Q., Chen, Z., Boroyevich, D., Ngo, K.D.T.: Assessment of encapsulants for high-voltage, high-temperature power electronic packaging. In: IEEE Electric Ship Technologies Symposium (ESTS). Alexandria, Virginia, USA, 2011.

5 Parr, C., Simonin, F., Touzo, B., Wohrmeyer, C., Valdelièvre, B., et al.: Impact of calcium aluminate cement hydration upon the properties of refractory castables, J. Tech. Assoc. Refract., **25**, 78 – 88, (2005).

6 Pöllmann, H.: Calcium aluminate cements - raw materials, differences, hydration and properties, Rev. Mineral. Geochem., **74**, [1], 1 – 82, (2012).

7 Seligmann, P., Greening, N.R.: New techniques for temperature and humidity control in X-ray diffractometry, J. PCA Res. Dev. Lab. 4, PCA Res. Dept. Bull., **143**, 2 – 9, (1962).

8 Jones, F.E., Roberts, M.H.: The System $CaO\text{-}Al_2O_3\text{-}H_2O$ at 25 °C (en), Build. Res. Stat., Current Paper Res. Ser. **1**, 27, (1962).

9 Smolczyk, H.-G.: Evaluating CAC concrete with X-ray analysis, in german, Betonstein-Ztg., **30**, 573 – 579, (1964).

10 Mishima, K.: Relation between the Hydration of Alumina Cement Mortars and their Strength in the Early Ages. In: 5th International Congress on the Chemistry of Cement, Tokyo, Japan, 1968.

11 Locher, F.W.: Cement: Principles of production and use, in German, Verl. Bau und Technik, Düsseldorf, 2000.

12 Wang, Y., Li, X., Zhu, B., Chen, P.: Microstructure evolution during the heating process and its effect on the elastic properties of CAC-bonded alumina castables, Ceram. Int., **42**, 11355 – 11362, (2016).

13 Han, B., Wang, P., Ke, C., Yan, W., Wei, Y., et al.: Hydration behavior of spinel containing high alumina cement from high titania blast furnace slag, Cement Concrete Res., **79**, 257 – 264, (2016).

14 Maaroufi, M.-A., Lecomte, A., Diliberto, C., Francy, O., Le Brun, P.: Thermo-hydrous behavior of hardened cement paste based on calcium aluminate cement, J. Eur. Ceram. Soc., **35**, 1637 – 1646, (2015).

15 Lee, W.E., Vieira, W., Zhang, S., Ahari, K.G., Sarpoolaky, H., et al.: Castable refractory concretes, Int. Mater. Rev., **46**, 145 – 167, (2001).

16 Klaus, S.: Quantification of CA hydration and influence of its particle fineness during early hydration of calcium aluminate cement, Dissertation, University of Erlangen-Nuremberg, Erlangen, Germany, 2015.

17 Goetz-Neunhoeffer, F.: Models for the hydration kinetics of calcium aluminate cement with calcium sulfate from a crystal-chemical and mineralogical point of view, in German, Erlanger Forschungen/Reihe B, Naturwissenschaften und Medizin, Erlangen, Germany, 2006.

18 Berthold, C., Presser, V., Huber, N., Nickel, K.G.: 1 + 1 = 3: coupling μ-XRD² and DTA, new insights in temperature-dependent phase transitions, J. Therm. Anal. Calorim., **103**, 917 – 923, (2011).

19 O'Connor, B.H., Raven, M.D.: Application of the rietveld refinement procedure in assaying powdered mixtures, Powder Diffr., **3**, 2 – 6, (1988).

20 Jansen, D., Goetz-Neunhoeffer, F., Stabler, C., Neubauer, J.: A remastered external standard method applied to the quantification of early OPC hydration, Cement Concrete Res., **41**, 602 – 608, (2011).

21 Funk, J.E., Dinger, D.R.: Predictive Process Control of Crowded Particulate Suspensions: Applied to Ceramic Manufacturing. Springer US, Boston, USA, 1994.

22 Telle, R., Salmang, H., Scholze, H.: Keramik: Mit 132 Tabellen (Ceramics: With 132 tables). 7th ed., Springer, Berlin, Heidelberg, New York, 260, 2007.

23 Reichling, K.: Determination and evaluation of the electrical concrete resistivity using geophysical methods, in German, 1st ed. Beuth Verlag GmbH, Berlin, 2015.

24 Wilkosz, D.E., Young, J.F.: Effect of moisture adsorption on the electrical properties of hardened portland cement compacts, J. Am. Ceram. Soc., **78**, 1673 – 1679, (1995).

25 Rouquerol, J., Rouquerol, F., Ganteaume, M.: Thermal decomposition of gibbsite under low pressures. II. formation of microporous alumina, J. Catal., **57**, 222 – 230, (1979).

26 Newman, J., Choo, B.S.: Advanced Concrete Technology 1: Constituent Materials. 1st ed. Elsevier Professional, 2/9, 2003.

27 Saalfeld, H.: Structures of hydrargillite and the intermediate phases during dehydration, in German, N. Jb. Mineral. Abh., **95**, 1 – 87, (1960).

28 IPC-TM-650, 2.6.3.3: Surface Insulation resistance, fluxes, International Standard, 2004

29 IEC 60747 – 9:2007: Semiconductor devices - Discrete devices – Part 9: Insulated-gate bipolar transistors (IGBTs), International standard, VDE Verlag, 2007.

30 IEC 60749 – 5:2017: Semiconductor devices - Mechanical and climatic test methods - Part 5: Steady-state temperature humidity bias life test, International Standard, VDE Verlag, 2017.

31 ZVEI LV324: Qualification of power electronic modules for components of motor vehicles, Edition 2014 – 02.